



Perfluorocarbon nanodroplet size, acoustic vaporization, and inertial cavitation affected by lipid shell composition *in vitro*

Phoebe J. Welch,¹  David S. Li,² Craig R. Forest,^{1,a)} Lilo D. Pozzo,³ and Chengzhi Shi^{1,a),b)} 

¹George W. Woodruff School of Mechanical Engineering, Georgia Institute of Technology, Atlanta, Georgia 30332, USA

²Philips, Bothell, Washington 98021, USA

³Department of Chemical Engineering, University of Washington, Seattle, Washington 98195, USA

ABSTRACT:

Perfluorocarbon nanodroplets (PFCnDs) are ultrasound contrast agents that phase-transition from liquid nanodroplets to gas microbubbles when activated by laser irradiation or insonated with an ultrasound pulse. The dynamics of PFCnDs can vary drastically depending on the nanodroplet composition, including the lipid shell properties. In this paper, we investigate the effect of varying the ratio of PEGylated to non-PEGylated phospholipids in the outer shell of PFCnDs on the acoustic nanodroplet vaporization (liquid to gas phase transition) and inertial cavitation (rapid collapse of the vaporized nanodroplets) dynamics *in vitro* when insonated with focused ultrasound. Nanodroplets with a high concentration of PEGylated lipids had larger diameters and exhibited greater variance in size distribution compared to nanodroplets with lower proportions of PEGylated lipids in the lipid shell. PFCnDs with a lipid shell composed of 50:50 PEGylated to non-PEGylated lipids yielded the highest B-mode image intensity and duration, as well as the greatest pressure difference between acoustic droplet vaporization onset and inertial cavitation onset. We demonstrate that slight changes in lipid shell composition of PFCnDs can significantly impact droplet phase transitioning and inertial cavitation dynamics. These findings can help guide researchers to fabricate PFCnDs with optimized compositions for their specific applications. © 2022 Acoustical Society of America.

<https://doi.org/10.1121/10.0014934>

(Received 16 May 2022; revised 17 August 2022; accepted 4 October 2022; published online 31 October 2022)

[Editor: Tyrone Michael Porter]

Pages: 2493–2504

I. INTRODUCTION

Lipid shelled microbubbles have been used as Food and Drug Administration (FDA) approved ultrasound contrast agents for several decades (Schneider 1999; Goertz *et al.*, 2007; Faez *et al.*, 2011). These gaseous structures ranging in size from 1 to 5 μm in diameter can be injected into the bloodstream and provide contrast for imaging the blood and tissue environment within the body. Furthermore, these microbubbles scatter ultrasound nonlinearly, which enables improved resolution and high contrast images with less tissue background signal (Goertz *et al.*, 2003). The use of microbubbles has enabled super-resolution ultrasound imaging of microvasculature in deep tissue structures, including the brain, muscles, and kidney (O'Reilly and Hynynen, 2013; Errico *et al.*, 2015; Song *et al.*, 2018; Yu *et al.*, 2018). Microbubbles can also be utilized for ultrasound-mediated drug delivery to blood clots and endothelial cells (Lentacker *et al.*, 2009; Lensen *et al.*, 2011). However, there are several drawbacks to microbubble contrast agents. Their size limits them to the bloodstream, and they cannot extravasate into tissue via inter-endothelial gaps in blood vessels

(Matsunaga *et al.*, 2012). Microbubbles are also unstable, only lasting minutes in the body before dissolution (Li *et al.*, 2018). In response to these issues, perfluorocarbon nanodroplets (PFCnDs) have been developed composed of similar materials, a lipid shell and perfluorocarbon core, but the nanodroplet core is liquid at room temperature, either because the perfluorocarbon core has a high bulk vaporization temperature or because the nanodroplets are in a superheated state (Kripfgans *et al.*, 2000; de Gracia Lux *et al.*, 2017). After exposure to an ultrasound pulse with sufficient energy, these nanodroplets phase-transition into gas microbubbles and can be ultrasonically imaged using nonlinear imaging techniques for improved contrast in the liquid or tissue environment (Sheeran *et al.*, 2011; Liu *et al.*, 2017; Jing *et al.*, 2020). Depending on environmental conditions and nanodroplet composition, such as the choice of perfluorocarbon used and temperature of the nanodroplet suspension, the PFCnDs can recondense back to a liquid state and undergo the expansion-recondensation cycle for repeated imaging purposes or can remain as gas microbubbles and be eliminated from the body within minutes to hours (Hannah *et al.*, 2016; Yu *et al.*, 2016; Yoon *et al.*, 2018). Due to their small size ($<300\text{ nm}$), they can extravasate into the leaky vasculature of tumors, which have large inter-endothelial gaps ranging from 380 nm to 2 μm (Rapoport *et al.*, 2011;

^{a)}Also at: Parker H. Petit Institute for Bioengineering and Bioscience, Georgia Institute of Technology, Atlanta, GA 30332, USA.

^{b)}Electronic mail: chengzhi.shi@me.gatech.edu

Yin *et al.*, 2012; Achmad *et al.*, 2018). PFCnDs also exhibit significantly better stability in circulation; compared to microbubbles whose lifespan is minutes long, PFCnDs with perfluoropentane (PFP) or perfluorohexane (PFH) cores remain stable in their liquid state for hours to days *in vitro* and *in vivo* (Williams *et al.*, 2013; Mountford and Borden, 2016; Li *et al.*, 2018; Ji *et al.*, 2022). PFCnDs can be utilized for targeted drug delivery and are superior for selective tissue ablation as they facilitate targeted, deep tissue heating without prefocal thermal delivery and damage to skin that occurs when using microbubbles (Rapoport *et al.*, 2011; Moyer *et al.*, 2015; Cao *et al.*, 2018; Goel *et al.*, 2021). Furthermore, due to their nanoscale size, functionalized PFCnDs can enter specific cell types via endocytosis for localized cell and tissue ablation; microbubbles are neither small nor stable enough for such applications (Ishijima *et al.*, 2019).

The process of PFCnDs transitioning from liquid nanodroplets to gaseous microbubbles from an ultrasound pulse is termed acoustic droplet vaporization (ADV). The pressure at which the nanodroplets undergo ADV can vary significantly based on several nanodroplet properties: nanodroplet diameter, core composition, and shell composition (Kawabata *et al.*, 2005; Aliabouzar *et al.*, 2019; Yarmoska *et al.*, 2019). These nanodroplet properties also affect inertial cavitation (IC) of PFCnDs, which is unstable bubble collapse with a broadband noise signature (Kang *et al.*, 2014). So long as the core bulk boiling point of PFCnDs is lower than the temperature of its surrounding environment, ADV and IC of PFCnDs are serially linked to one another, with ADV occurring first to form gas microbubbles before IC occurs in those microbubbles, although ADV and IC pressure thresholds can overlap (Schad and Hynynen, 2010; Wu *et al.*, 2021). Preventing IC from occurring while using PFCnDs and microbubbles as ultrasound contrast agents is particularly crucial for *in vivo* imaging due to its potential to cause significant damage to surrounding tissues; therefore, having a large pressure difference between ADV onset and IC onset is of importance to medical imaging researchers.

Previous studies have demonstrated that nanodroplet size, stability, and image contrast are heavily reliant on their lipid shell composition. Mountford *et al.* (2015) studied PFCnDs composed of phospholipid shells with acyl lengths ranging from C14 to C24 and noted that the energy required to induce phase transitioning linearly trended with increasing acyl length chain (Mountford *et al.*, 2015). Yarmoska *et al.* (2019) showed that increasing the ratio of PEGylated to non-PEGylated lipids in photoacoustic PFCnDs yielded smaller nanodroplets with smaller standard deviations and stronger photoacoustic signals compared to PFCnDs with higher ratios of non-PEGylated to PEGylated lipids (Yarmoska *et al.*, 2019). Chattaraj *et al.* (2016) noted that different combinations of saturated and unsaturated phospholipids in combination with cholesterol affected the B-mode acoustic intensity of PFH-core PFCnDs, possibly due to the clustering and phases of the lipid shells (Chattaraj

et al., 2016). From these papers, slight changes in lipid shell composition, like the carbon chain lengths or the ratio of different phospholipids and surfactants, can significantly impact size distribution and ultrasound image contrast. However, there is limited research on how the lipid shell impacts ultrasonically induced phase transitioning of PFCnDs and whether the shell composition influences the IC threshold.

In this work, we investigated the effect of varying lipid shell composition of PFCnDs on nanodroplet size, ADV and IC onset, and the ultrasound intensity and duration of phase-transitioned PFCnDs by varying the ratio of PEGylated and non-PEGylated lipids, which are commonly used for fabricating lipid shelled ultrasound contrast agents. These nanodroplets had cores composed of either PFP, PFH, or a combination of the two perfluorocarbons. These perfluorocarbons were selected to encourage recondensation of the phase-transitioned nanodroplets; using perfluorocarbons with lower boiling points like perfluorobutane (PFB) (boiling point = -2°C) would result in microbubbles unable to recondense in the water bath heated to 37°C . PFCnDs fabricated via spontaneous nucleation were suspended in agarose hydrogels and insonated using a focused ultrasound transducer. A linear array transducer, synchronized to the focused ultrasound transducer, captured B-mode images and radio frequency (RF) data of the insonated PFCnDs, which were used to study the vaporization and cavitation dynamics of the nanodroplets, respectively.

II. MATERIALS AND METHODS

A. Nanodroplet fabrication and size-exclusion techniques

Nanodroplets were fabricated using a spontaneous nucleation method as previously described by Li *et al.* (2018). This fabrication method was used as it can consistently create small ($<250\text{ nm}$ diameter), uniform PFCnDs with no need for specialized equipment or harmful chemicals like chloroform. Lipid stock solutions were created with varying molar ratios of 1,2-dipalmitoyl-*sn*-glycero-3-phosphocholine (DPPC) and *N*-(carbonyl-methoxypolyethyleneglycol 2000)-1,2-distearoyl-*sn*-glycero-3-phosphoethanolamine (DSPE-PEG₂₀₀₀) (NOF America Corp., White Plains, NY) dissolved in 190 proof ethanol. These lipid stocks were composed of 90:10 DPPC:DSPE-PEG₂₀₀₀, 50:50 DPPC:DSPE-PEG₂₀₀₀, or 10:90 DPPC:DSPE-PEG₂₀₀₀. The final concentration of lipids in these solutions was $2\ \mu\text{M}$. One milliliter of each stock solution was added to a microcentrifuge tube, and perfluorocarbons—either PFP (FluoroMed L.P., Round Rock, TX), PFH (FluoroMed L.P.), or a combination of the two—were added to the lipid solutions until the solution was saturated with perfluorocarbon, as characterized by a noticeable pellet of undissolved perfluorocarbon collected at the bottom of the microcentrifuge tube. The ratios of PFP:PFH used in these experiments were as follows: 100:0, 90:10, 70:30, 50:50, and 0:100. We ultimately want to create nanodroplets that will phase-transition under diagnostically safe acoustic

pressures [mechanical index (MI) below 1.9] while also being capable of recondensing back into a liquid state, so the nanodroplets fabricated tended to have a higher ratio of PFP to PFH, and 30:70 and 10:90 PFP:PFH nanodroplets were not included in this study (Sen *et al.*, 2015). A 2% solution of DiI (a lipophilic fluorescent tracer; MilliporeSigma, St. Louis, MO) dissolved in ethanol was added to the lipid/perfluorocarbon solution. DiI was used in all experiments as these PFCnDs with this composition will later be used in cell and tissue imaging studies. The microcentrifuge tube was vortex mixed and sonicated until the solution was cloudy. At this point, the solution was left for 20 min for additional undissolved perfluorocarbon to fall out of solution. 50 μl of this lipid/PFC/DiI solution were added to 100 μl of lipid stock solution in microcentrifuge tubes. Then 850 μl of a 7:2:1 water:propylene glycol:glycerol (MilliporeSigma) solution was added to the diluted lipid/PFC solutions. The rapid addition of this hydrophilic miscible solution caused the dissolved lipids and PFC to spontaneously nucleate into very small droplets with the lipid encapsulating the PFC “core” to form a stable dispersion in a process called spontaneous emulsification. From here, all samples were centrifuged for 80 min at $6000 \times g$, the supernatant was removed, and the pellet of nanodroplets was resuspended in phosphate buffered saline (PBS) (Corning Inc., Corning, NY).

To test the optimal filtration technique, we created several batches of nanodroplets made from the same lipid shell stock through the spontaneous nucleation method. These solutions were then either passed through a 450 nm mesh filter, centrifugated, or left undisturbed. The size and concentration of these nanodroplet solutions were measured the same day as the ultrasound experiments, which was typically ~ 24 h after fabrication. These were the four conditions we tested:

- Control: No changes to nanodroplet solution after resuspending in PBS.
- Size-exclusion centrifugation: The nanodroplet solution was spun down at $300 \times g$ for 5 min to allow the large nanodroplets to settle to the bottom of the tubes. The supernatant was recovered, and this process was repeated three times.
- Gravity filtration: A 450 nm mesh filter (Corning) was attached to a syringe. The nanodroplet solution was loaded into the syringe and allowed to pass through the filter via gravity.
- Pressure filtration: A 450 nm mesh filter was attached to a syringe, and after the nanodroplet solution was loaded, the syringe plunger was depressed slowly until the entire nanodroplet solution passed through the filter.

On the day of experiments (~ 24 h post-fabrication), the concentration and size of the nanodroplets were measured using a NanoSight300 (Malvern Panalytical, Worcestershire, UK). The concentration for each PFCnD stock was noted and used to create appropriate dilution factors such that the same quantity of each type of PFCnDs was suspended in agarose gels. PFCnD solutions were stored at 4°C until use.

B. Ultrasound imaging and calibration

All experiments took place in a water bath heated to 37°C . Nanodroplets were suspended in a 1% agarose gel (MilliporeSigma) to a final concentration of 1×10^8 nanodroplets/ml ($4.2 \times 10^{-5}\%$, v/v) and loaded into thin-walled plastic containers. A focused single-element transducer (H-101, Sonic Concepts Inc., Bothell, WA) operating at its third harmonic frequency of 3.5 MHz (determined by performing a parametric frequency sweep between 3 and 4 MHz) was aligned with the nanodroplet gel sample. The single-element transducer was connected to a function generator (Agilent E4422B, Santa Clara, CA) and amplified with an RF power amplifier (325 LA, E&I Ltd., Rochester, NY). A coupling cone was placed on the single-element transducer to align the focus of the transducer to the nanodroplet sample. This single-element transducer setup was used to initiate droplet vaporization in the nanodroplet sample. Orthogonal to the nanodroplet sample was a linear array transducer (L7-4v, Philips, Bothell, WA) operating at its center frequency of 5 MHz and transmitting plane waves at a frame rate of 3500 Hz, which captured B-mode images of the vaporized nanodroplets above the focal spot of the focused ultrasound transducer [Fig. 1(a)]. Data were acquired using a Research Ultrasound system (Vantage 256, Verasonics, Inc., Kirkland, WA) running a custom MATLAB script that synchronized the focused ultrasound pulse with the captured B-mode image. Thirty pre-activation B-mode image frames were collected as background signal, and then the single-element transducer was triggered by the Vantage 256 to emit a 20-cycle burst sine wave at a specified pressure output to initiate ADV in the nanodroplet-loaded agarose gel, followed by 400 post-ADV B-mode frames. A 20-cycle burst was selected to keep the transmission duty cycle well below 10%. The 20-cycle burst was also selected to simultaneously phase-transition a high proportion of PFCnDs while preventing IC, as longer bursts (20+ cycles) have greater chances of phase-transitioning more nanodroplets at lower insonation pressures while also risking IC at lower pressures (Chen *et al.*, 2003; Reznik *et al.*, 2011; Guo *et al.*, 2013; Wu *et al.*, 2021). This activation and imaging sequence was repeated 20 times per pressure output, starting at the lowest pressure (2 MPa) output and gradually ramping the pressure amplitude from 2 to 9.5 MPa PNP (MI = 1–5). Data were stored as both raw RF data (for IC detection) and B-mode image frames (for ADV analysis). The single-element transducer pressure output was calibrated prior to experiments using an HGL-0200 capsule hydrophone (ONDA Corp., Sunnyvale, CA), with RF data collected in LabVIEW 2019 (National Instruments, Austin, TX) and analyzed in MATLAB 2020a (MathWorks, Natick, MA). Voltage to pressure calibration of the single-element transducer was performed with the coupling cone and a thin (~ 1 mm) layer of 1% agarose gel in front of the transducer to simulate experimental conditions and account for any attenuation caused by the coupling cone and gel setup.

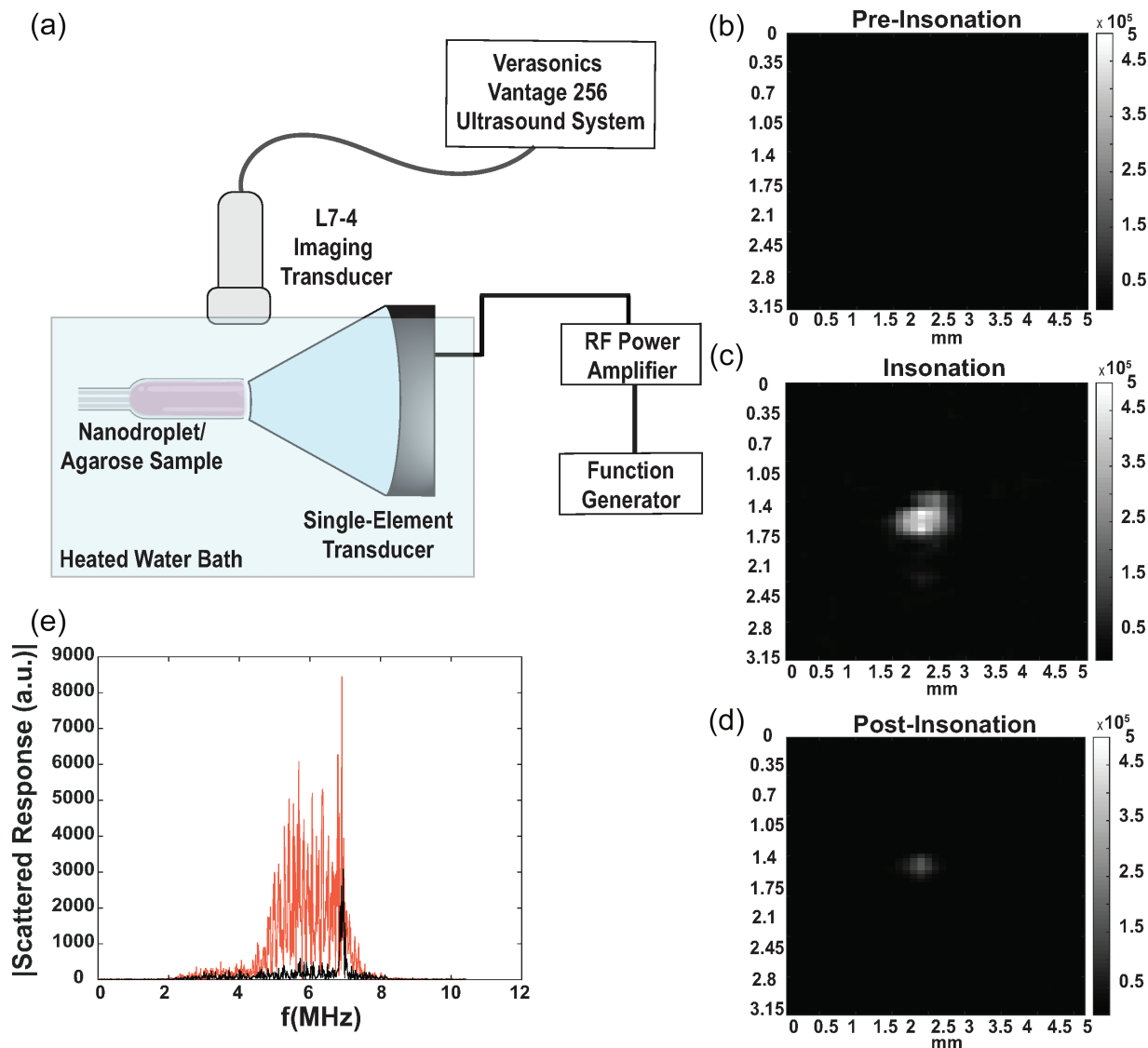


FIG. 1. Methods used for B-mode image and RF data collection for ADV and IC characterization. (a) Overview of experimental setup. (b), (c), (d) Representative B-mode images of PFCnD phase transitioning and recondensation/dissolution before, during, and after insonation, respectively. Nanodroplets used in these images are 50:50 lipid shelled, 50:50 PFP:PFH nanodroplets. (e) Fourier transform of insonated PFCnDs at 2 MPa peak negative activation pressure (black line, no ADV or IC) and at 9 MPa peak negative activation pressure (red line, evidence of IC).

C. ADV characterization

ADV was quantified by measuring the mean echo power (MEP) of the focal spot within the imaging window, as described by Fabiilli *et al.* (2009) and used in later applications. The MEP is calculated by summing the squared amplitude of all pixel intensities within an imaging window and then normalized by the window area as follows:

$$MEP(m) = \frac{1}{MN} \sum_{i=1}^M \sum_{j=1}^N A_{i,j}^2, \quad (1)$$

where m is the frame number with dimensions M, N , and A is the amplitude at pixel i, j . The MEP of ultrasound frames just after insonation [Fig. 1(c)] will be significantly higher than frames preceding the activation event [Fig. 1(b)] if the activating ultrasound sequence was powerful enough to

induce ADV. The MEP would also significantly decrease post-insonation after a short period if PFCnDs either recondensed or dissolved into the surrounding scaffold [Fig. 1(d)]. We calculated the average MEP of 20 post-activation frames, ignoring the two frames immediately after the activating ultrasound sequence to prevent signal from the focused ultrasound transducer from interfering with our calculations.

The MEP calculations were used to analyze the duration and intensity of vaporized nanodroplets. MEP duration was characterized as the number of post-activation frames where the MEP was elevated above a threshold value, $20 \times MEP_{Avg, \text{ pre-activation}}$, where $MEP_{Avg, \text{ pre-activation}}$ is the average MEP value of the 30 pre-activation frames before the vaporization pulse is triggered. This threshold was determined by measuring the average and standard deviation of the pre-activation frames and selecting a multiplier that

would ensure the MEP signal measured in the post-activation frames was caused by phase-transitioning PFCnDs and not background noise. Usually, the MEP of B-mode images of ADV was several orders of magnitude higher than frames containing no ADV, so increasing or decreasing the multiplier for the threshold value slightly (e.g., ± 5) does not significantly affect the measurement. MEP intensity comparisons between different groups of PFCnDs were made by determining the maximum MEP induced by the activation pulse per activation and imaging sequence.

D. IC characterization

IC was determined by analyzing the RF data received by the imaging transducer immediately after the phase-transitioning ultrasound pulse. The RF data collected by the four elements of the linear array transducer located directly above the focal spot of the single-element transducer was analyzed by taking the fast Fourier transform and analyzing the signal amplitude between 4 and 6 MHz. This frequency window was selected because it did not contain any of the second harmonic signal coming from the nanodroplets caused by the single-element transducer (~ 7 MHz) and could be used as a region to characterize the noise floor. Since IC is typically measured by broadband acoustic emission, we could use this frequency region to gauge if there was an elevated noise floor after the activation ultrasound pulse. Transducer elements were specifically selected to be located above the focus spot of the activation pulse, as determined by analyzing the B-mode image data. The signal from the lowest activation pulse pressure was used as the noise floor baseline measurement. A threshold was empirically selected in a similar manner as used in [Fabiilli et al. \(2009\)](#) to distinguish an IC event from background noise caused by the insonating focused ultrasound transducer. The threshold for IC detection was set as

$$NF_{\text{sample}} > NF_{\text{base}} + 3 * \delta_{NF_{\text{base}}}, \quad (2)$$

where NF_{sample} is the noise floor of the sample of interest [Fig. 1(e), red line], NF_{base} is the noise floor of the PFCnD sample at the lowest insonation pressure (2 MPa PNP), and $\delta_{NF_{\text{base}}}$ is the standard deviation of the noise floor at the lowest insonation pressure [Fig. 1(e), black line]. The threshold for IC detection is quite low so that the IC analysis is very sensitive to any potential IC events in the nanodroplet samples.

E. Statistical analysis

ADV and IC data were plotted using MATLAB, and sigmoidal best-fit curves were fitted to the scatterplot data. The custom equation for the sigmoidal curve is $y = a + (b - a) / [1 + (x/c)^d]$, where x is the pressure value; y is either the cavitation probability or ADV intensity; a and b are the maximum and minimum y -values, respectively; c is the x -value at the y -midpoint; and d is the slope at c ([Fabiilli et al., 2009](#)). These sigmoidal curves were used to determine

the onset of ADV and IC. ADV onset was characterized by the appearance of ultrasound contrast immediately after the insonating pulse by the focused ultrasound transducer, caused by the phase transitioning of the PFCnDs. This appearance of ultrasound contrast correlates well with the x -value at the y -midpoint of the sigmoidal curve. IC onset is defined as the 50% crossing of the sigmoid fit on the cavitation curve ([Li et al., 2018](#)). Box plots and statistical analysis were conducted in R Studio. One-way analysis of variance (ANOVA) and Tukey's t -test were used to determine statistical significance in variances between different nanodroplet compositions.

III. RESULTS AND DISCUSSION

A. Nanodroplet filtration

Nanodroplet composition impacts the size distribution of the resulting nanodroplets, which can significantly influence ADV and IC thresholds ([Ferri et al., 2021](#)). If there are large nanodroplets present in the nanodroplet suspension, ADV can be observed at relatively low pressures as nanodroplets with larger diameters require lower pressures to vaporize than those with smaller diameters due to superharmonic focusing ([Kripfgans et al., 2004](#); [Shpak et al., 2014](#); [Aliabouzar et al., 2019](#)). To eliminate particularly large nanodroplets, centrifugation is commonly used to separate large, coalesced nanodroplets from the rest of the sample ([Mercado et al., 2016](#)). However, this size-exclusion technique has not been extensively compared to other separation methods, such as mesh filtration. We sought to optimize a simple but effective nanodroplet filtration method to create nanodroplet solutions of uniform, monodisperse nanodroplets by passing our nanodroplet suspensions through a 450 nm mesh filter. We selected 450 nm mesh filters for our filtration studies knowing that mesh filters are not perfectly monodisperse, and if we used filters with an average pore size closer to our initial average nanodroplet diameter (~ 220 nm), we would risk excluding a much higher proportion of nanodroplets and, thus, significantly reduce the quantity of nanodroplets in our solutions ([Ullmann et al., 2019](#)). The control sample of nanodroplets, which did not undergo any size-exclusion separation technique, had the largest mean diameter and standard deviation in diameter distribution amongst the samples [Figs. 2(a) and 2(c)]. The gravity filtered and pressure filtered nanodroplets yielded the smallest average diameter without significantly reducing the concentration of the sample [Figs. 2(b) and 2(c)]. To eliminate the risk of including large (>450 nm) nanodroplets in our study, all nanodroplet samples were pressure filtered before being used for ultrasound imaging in subsequent experiments.

Nanodroplets passed through a 450 nm mesh filter had significantly smaller diameters than non-filtered and centrifugated nanodroplets. At surface level, these findings seem obvious, but in reality, the results are somewhat surprising because it has been hypothesized that pushing lipid shelled PFCnDs through a mesh filter can cause some nanodroplets

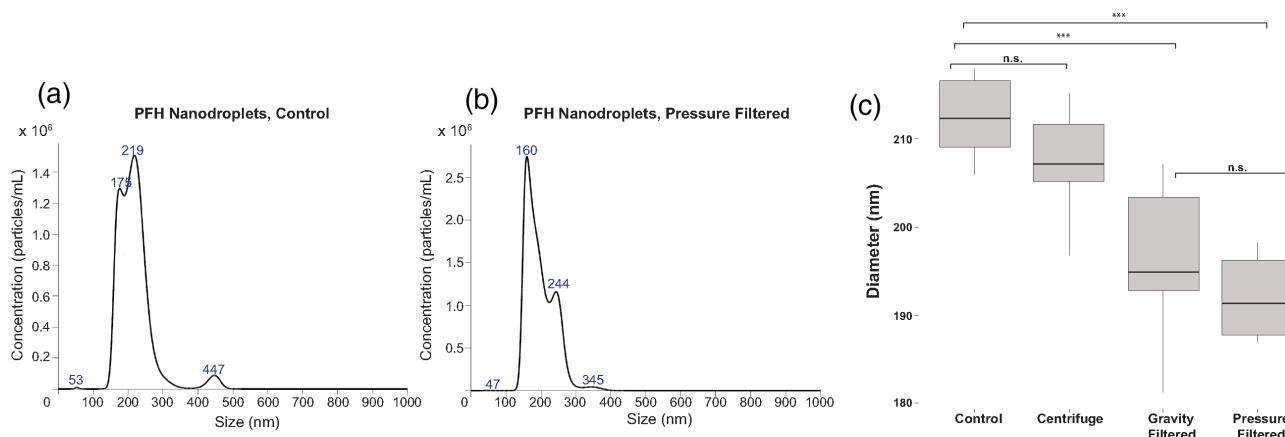


FIG. 2. (Color online) Size-exclusion techniques on PFCnD diameters. (a) Size distribution of PFCnDs with a PFH core with no size separation technique applied. Average diameter of these droplets was 217.9 ± 52.2 nm, 10^{10} nanodroplets/ml. (b) Size distribution of PFCnDs with a PFH core after passage through a syringe fitted with a 450 nm mesh filter. Average diameter of these droplets 197.5 ± 41.1 nm, 10^{10} nanodroplets/ml. (c) PFCnDs passed through a 450 nm filter yielded nanodroplets with the smallest diameters, compared to centrifugation techniques and unmodified (control) nanodroplet samples. $n = 6$.

to break open and coalesce with nearby droplets (Paproski *et al.*, 2016). This theory is still possible, though perhaps the large nanodroplets formed via coalescing are less stable than the smaller ones and either evaporate or coalesce and sediment within the 24h period between fabricating the PFCnDs and measuring their size and concentration. The more likely reason that mesh filtered PFCnDs tend to have smaller average diameters is because any nanodroplets greater than the mesh pore size (in this case, 450 nm) are excluded from size measurements and do not contribute to the diameter calculations by the NanoSight 300. The mesh filtered nanodroplets may have a slightly larger standard deviation compared to the centrifugated and control nanodroplets either because some nanodroplets are fractured by the filter and the lipid shell fragments form very small (<100 nm) liposomes containing no perfluorocarbons or

because some of the nanodroplets have excess lipid shell that is shed as they pass through the filter and form liposomes (Borden *et al.*, 2005).

Next, we investigated how the lipid shell composition impacts nanodroplet size distribution. PFCnDs with a PFH core were passed through a 450 nm mesh filter attached to a 1 ml syringe with the plunger gently applied to eliminate larger nanodroplets. Based on three different batches of PFCnDs, nanodroplets with a 10:90 ratio of DPPC:DSPE-PEG₂₀₀₀ were significantly larger than 50:50 and 90:10 lipid shelled nanodroplets [Fig. 3(a)]. There was no significant difference in nanodroplet diameter is observed when PFCnDs are grouped by core composition [Fig. 3(b)], indicating that the lipid shell, rather than core composition, influences nanodroplet size distributions.

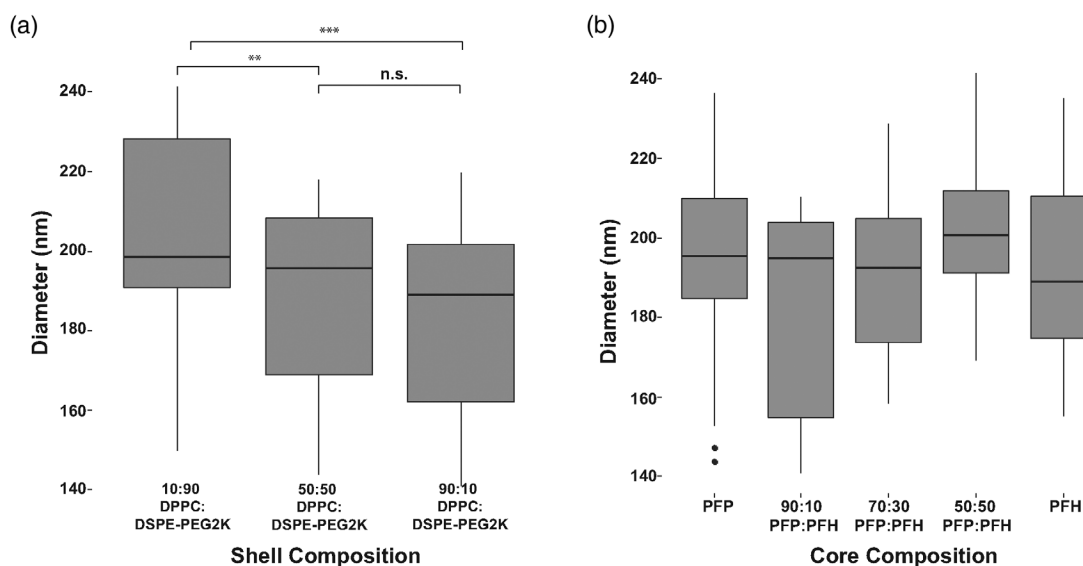


FIG. 3. PFCnD size distribution vs lipid shell composition. (a) 10:90 lipid shelled PFCnDs had notably larger nanodroplets across all experiments and core compositions ($n = 27$). (b) Grouping nanodroplets with different lipid shell compositions together based on perfluorocarbon core, no significant difference in diameter was observed amongst PFCnDs with different core compositions, indicating changes in PFCnD sizes are linked to shell composition ($n = 9$).

B. ADV intensity vs shell composition

Ultrasound B-mode image intensity caused by the phase transitioning of the PFCnDs is critical for medical imaging applications, as PFCnDs that produce a stronger acoustic signal are easier to locate *in vivo*. The intensity of the resulting image contrast produced after ADV was quantified by calculating the MEP in the focal region [Fig. 4(a)]. Once the insonating pressure from the single-element transducer reached a certain threshold, a noticeable bubble cloud would appear in the transducer’s focal region. As the transducer increased above this pressure, the bubble cloud intensity increased, indicating a greater proportion of nanodroplets were phase-transitioned in the focal region and yielding a higher MEP. This trend continued until the insonating pressure reached 7–7.5 MPa peak negative pressure (PNP) (MI = 3.75–4), at which point the maximum number of PFCnDs were phase-transitioned during each insonating pulse. Analyzed across three experimental periods with separate batches of nanodroplets, the 50:50 lipid shelled PFCnDs exhibited significantly stronger ADV intensities than the 10:90 and 90:10 lipid shelled nanodroplets [Fig. 4(b)]. The 90:10 and 10:90 non-PEGylated:PEGylated PFCnDs had comparable MEP values.

These insonating pressures exceed the recommended pressures used in medical ultrasound and are required in this study due to the agarose hydrogel environment whose matrix suppresses some nanodroplet expansion (as opposed to an all-liquid environment more commonly used in nanodroplet studies). The ADV threshold can be easily modified by changing the core composition to contain lower boiling point perfluorocarbons, such as PFB, and increasing the number of cycles per insonating pulse.

The increased B-mode intensity in nanodroplets with a 50:50 lipid shell ratio of non-PEGylated:PEGylated lipids could be caused by several factors. It is possible that these 50:50 nanodroplets have improved vaporization efficiency

compared to other nanodroplet compositions, so a larger proportion of nanodroplets expand with each insonating pulse. The cause of this improved vaporization efficiency may be the packing structure and distribution of the two phospholipids in the nanodroplet shell. In one study of multi-component phospholipid micelles by Viitala *et al.* (2019), the authors noted that increasing the ratio of DSPE-PEG₂₀₀₀ in the DPPC:DSPE-PEG₂₀₀₀ liposomes from ~10% DSPE-PEG₂₀₀₀ to 50% DSPE-PEG₂₀₀₀ caused a shape change from bicelles to slightly elongated micelles (Viitala *et al.*, 2019). DPPC:DSPE-PEG₂₀₀₀ lipid shelled nanodroplets have small domains of only DPPC or DSPE-PEG₂₀₀₀, creating a solid-liquid ordered phase coexistence, as detailed in Chattaraj *et al.* (2016). The authors also noted that increasing the PEG concentration in these droplets from 3% mol to 20% mol caused a significant increase in acoustic signal, likely because PEGylated lipids are typically included in lipid shelled nanodroplets for increased steric stabilization and perhaps because this lipid shell organization, with distinct regions of DPPC and DSPE-PEG₂₀₀₀, causes nanodroplets to phase-transition well without IC or dissolution into the surrounding medium. Our results agree with Chattaraj *et al.* in that increasing the ratio of PEGylated lipids from 10% mol to 50% mol yielded a significantly stronger acoustic response post-ultrasound insonation. However, the addition of too much PEGylated lipid could create steric hindrance issues and/or create lipid shells too stiff for efficient nanodroplet expansion, hence, why our 10:90 DPPC:DSPE-PEG₂₀₀₀ nanodroplets had lower acoustic signal overall.

Another potential cause of stronger acoustic intensity is that the 50:50 lipid shelled nanodroplets yield larger gaseous microbubbles after insonation compared to the other two compositions. PFCnDs will typically yield microbubbles that are 3–5 times larger in diameter than their liquid, condensed form, with smaller nanodroplets forming proportionally

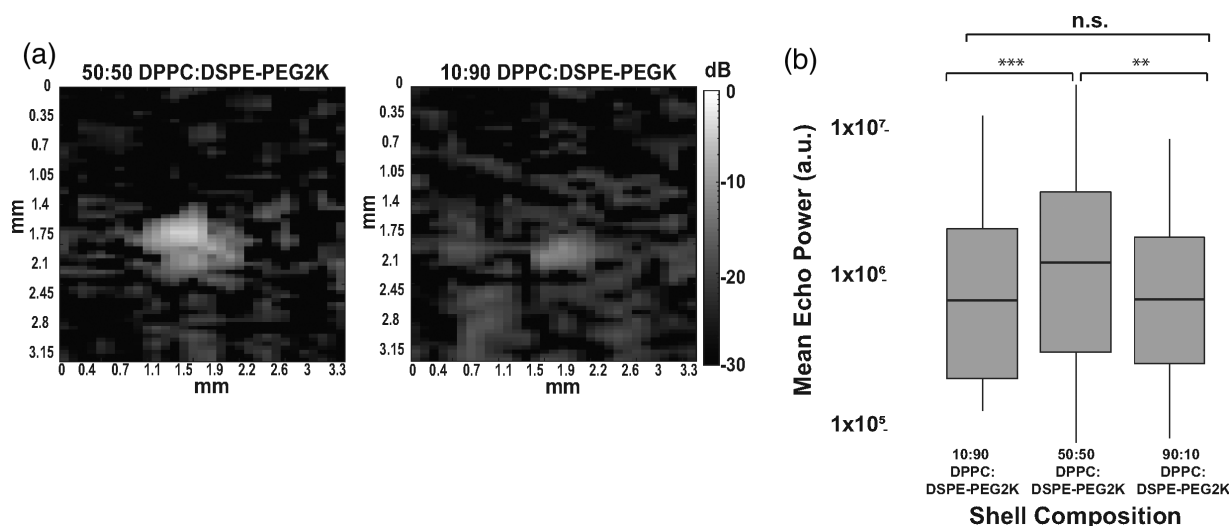


FIG. 4. Comparison of lipid shell PFCnD B-mode image intensity. (a) B-mode images of 50:50 lipid shell and 10:90 lipid shell PFCnDs after insonation at the same PNP (9 MPa). (b) PFCnDs with a 50:50 lipid shell consistently exhibited greater ultrasound contrast across all core compositions and nanodroplet batches.

smaller microbubbles due to increased Laplace pressure (Sheeran *et al.*, 2011). The interfacial tension differences between the lipid shell and perfluorocarbon core may impact the Laplace pressure and shell stiffness, which could affect ADV conversion efficiency and the responsiveness of the resulting bubbles for the lipid shelled PFCnDs. Thus, the 50:50 lipid shelled nanodroplets may stably expand to a larger microbubble diameter than the other compositions, or a greater proportion of the 50:50 lipid shelled nanodroplets expand with each insonating ultrasound pulse, providing greater ultrasound contrast. Confirmation of these theories would require an experimental setup similar to that in Seda *et al.* (2015), in which PFCnDs were placed above a microscope objective, and the resulting bubble clouds post-insonation were optically observed (Seda *et al.*, 2015). Further research on the ideal ratio of PEGylated to non-PEGylated lipids in PFCnDs must be conducted to determine the ideal shell ratio, but among the nanodroplet compositions used in this study, 50:50 lipid shelled PFCnDs would be the ideal ultrasound contrast agent to use in imaging applications where stark image contrast is required.

Although using nanodroplets with a higher PEGylated lipid ratio may yield improved ultrasound contrast, one area of concern is potential bioeffects caused by lipid shell composition. PEG is a common additive to a variety of nanomaterials used to increase *in vivo* stability (Niidome *et al.*, 2006; Diaz *et al.*, 2018). Studies investigating the use of PFCnDs *in vivo* have used a variety of PEG ratios in lipid shells, even up to 90% PEGylated lipids, with no reported ill effect (Xiang *et al.*, 2019; Yarmoska *et al.*, 2019; Sheng *et al.*, 2021). While using PFCnDs with various PEG ratios appears to be safe for one-time, short-term experiments, long-term and repeated administration of PFCnDs, especially those with higher PEG ratios, has not been thoroughly investigated and could potentially lead to nanodroplet build-up within certain organs,

increased clearance from the circulatory system, and cytotoxicity. Researchers studying PEGylated liposomes for drug delivery have noted that repeated injections of PEGylated liposomes at certain concentrations lead to accelerated blood clearance after the first injection due to anti-PEG IgM-mediated activation (Ishida *et al.*, 2007; Ichihara *et al.*, 2010; Suzuki *et al.*, 2012). Additionally, high PEG ratios can prevent nanoparticle uptake into cells, which may be an issue if the desired use of these PFCnDs is to use them for targeted intracellular uptake (Verhoef and Anchordoquy, 2013; Pozzi *et al.*, 2014). Researchers should consider these potential effects that may result *in vivo* when creating PFCnDs and design the lipid shell composition appropriately based on the desired application. Researchers should also use caution if utilizing these PFCnDs for long durations or repeated injections as there may be unknown cytotoxic effects or increased immune activation that result from repeated use.

C. ADV duration vs shell composition

The duration for which vaporized PFCnDs remained in their gaseous state was calculated by measuring the number of frames in which the MEP in ultrasound frames post-ADV was elevated above the threshold value $20 \times \text{MEP}_{\text{Avg, pre-activation}}$. PFCnDs composed of a 10:90 DPPC:DSPE-PEG₂₀₀₀ lipid shell had the briefest duration in the gaseous state across all nanodroplet batches and core compositions [Fig. 5(a)]. There was no significant difference in ADV duration between the 50:50 and 90:10 lipid shelled PFCnDs. Post-insonation peaks in MEP were observed in the same nanodroplet samples after multiple insonation events, even in nanodroplets with boiling points below the environment temperature, suggesting nanodroplet recondensation [Fig. 5(b)].

The disappearing ultrasound signal after phase transitioning can be attributed to several factors. The perfluorocarbon

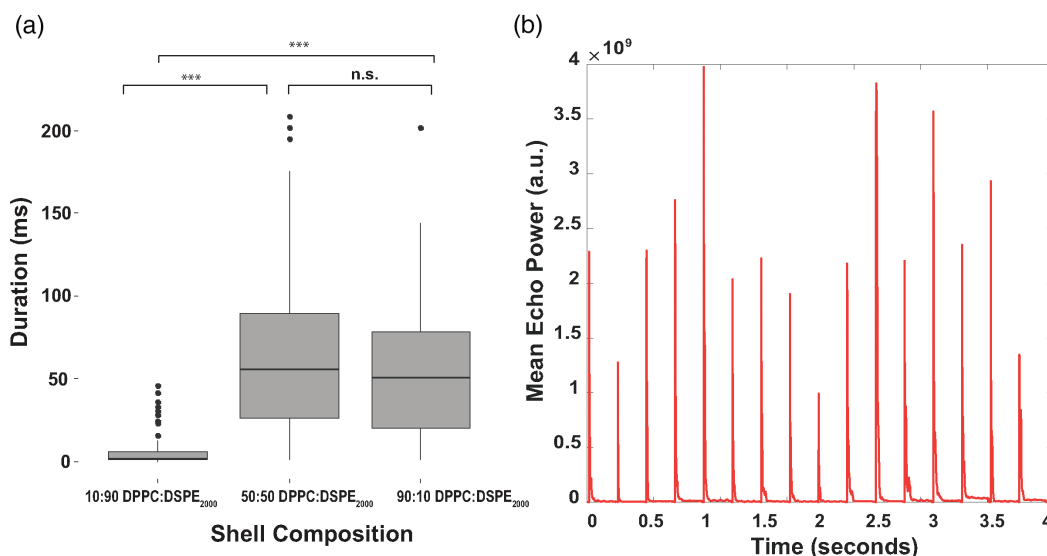


FIG. 5. Representative duration data from one dataset depicting the differences in MEP across all nanodroplet types. (a) 10:90 lipid shell nanodroplets exist as gaseous microbubbles for significantly shorter periods compared to both 90:10 and 50:50 lipid shell nanodroplets across all core compositions. (b) MEP vs time in PFP nanodroplets with a 50:50 non-PEGylated:PEGylated lipid shell, insonated at maximum operating pressure (9.5 MPa).

core composition can significantly impact whether nanodroplets can recondense or dissolve into the surrounding environment. Nanodroplet recondensation has been observed in nanodroplets composed of both PFP and PFH cores (Hannah *et al.*, 2016; Ishijima *et al.*, 2016; Luke *et al.*, 2016; Yu *et al.*, 2016; Yoon *et al.*, 2018), so it is possible that many of the nanodroplets within the PFCnD samples tested in these experiments are recondensing to a liquid state after insonation, as observed in Fig. 5(b). The sustained signal intensity across all subsequent insonating pulses, even at very high pressures, supports this claim. Furthermore, the agarose matrix in which the PFCnDs are suspended can encourage recondensation rather than fragmentation, whereas in flow tube phantoms, there tends to be a loss in ultrasound signal as the liquid nanodroplet suspension is repeatedly subjected to high intensity ultrasound pulses (Yoo *et al.*, 2018). Differences in interfacial properties of the lipid shelled PFCnDs could significantly impact the recondensation of the vaporized bubbles, with the 10:90 lipid shelled nanodroplets exhibiting the greatest interfacial forces and the 50:50 lipid shelled nanodroplets possessing weaker interfacial forces. The high proportion of PEGylated lipids in the 10:90 PFCnDs could also be the cause of rapidly disappearing acoustic signal as the PEG creates stiffer encapsulating shells, encouraging fracturing and/or rapid recondensation of the nanodroplets. Last, some PFCnDs, especially those composed of a core with a lower vaporization temperature threshold, may fragment post-phase transitioning due to being in an environment above the vaporization point of the core and possessing an unstable lipid shell, despite their suspension in agarose gel (de Jong *et al.*, 2000; Huynh *et al.*, 2015).

D. Pressure differential between ADV onset and IC onset

We also investigated the onset of ADV and IC in all PFCnD samples. IC was characterized by a significant increase in the noise floor directly after insonation by the single-element transducer compared to the noise floor of the lowest insonation pressure used (2 MPa). From here, the pressure difference between ADV onset (insonation pressure at which nanodroplets begin to phase-transition) and IC onset (characterized as 50% cavitation probability) was calculated across all samples. PFCnDs with a 50:50 lipid shell ratio had the largest pressure difference between when ADV was noticeable and when IC surpassed the vaporization threshold compared to 10:90 and 90:10 lipid shelled nanodroplets, as exhibited by the representative plots in Figs. 6(a)–6(c). This trend was observed across all nanodroplet samples of various sizes and core composition, and the pressure differential was considerably larger in nanodroplets with smaller diameters [150–180 vs 200–250 nm; Fig. 6(d)].

The differential between ADV and IC onset is an important metric for both imaging and therapeutic applications. For ultrasonic imaging of these contrast agents *in vivo*, IC can be detrimental to surrounding cells and tissues; inducing ADV without triggering IC, therefore, is critical. Creating PFCnDs with the lowest possible ADV

threshold is crucial in diagnostic imaging to enable phase transitioning without using insonating pressures above the FDA's MI threshold for *in vivo* applications. Contrary to this, damaging tissues and cells via IC can be the goal of using ultrasonically triggerable PFCnDs, so nanodroplets with a lower IC threshold are ideal, and the pressure difference between ADV onset and IC onset is negligible. Based on these considerations, 50:50 lipid shelled PFCnDs would be ideal contrast agents for theranostic applications; these droplets exhibited the greatest ADV-to-IC onset pressure differential and highest contrast to noise and could, thus, facilitate both ultrasound imaging (ADV) and ultrasound-induced drug released or localized tissue ablation (IC). However, the perfluorocarbon cores used in this paper yielded PFCnDs with ADV thresholds above the FDA's MI limit. Changing the perfluorocarbon core to include perfluorocarbons with lower vaporization temperatures (e.g., PFB) can bring the ADV threshold to biologically safe pressures.

It is important to consider that the window between ADV and IC is quite narrow, even for the 50:50 lipid shelled PFCnDs. This narrow pressure differential has been observed in other works and has implications for utilizing PFCnDs safely for *in vivo* applications (Wu *et al.*, 2021). Our findings demonstrate that the ADV-to-IC pressure differential is larger for PFCnDs with smaller diameters, but one problem with small nanodroplets (diameters <200 nm) is that they require very high insonation pressures exceeding MI limits compared to larger nanodroplets. Researchers have developed ways to lower and control both ADV and IC thresholds by using unique transducer configurations or ultrasound standing waves, but future work should investigate whether these techniques can be used to create a greater ADV-to-IC differential, whether these techniques can be used to insonate and phase-transition nanodroplets with sub-200 nm diameters, and whether these techniques are applicable *in vivo* (Guo *et al.*, 2017; Xu *et al.*, 2018).

It is important to note that all experiments in this paper were conducted in tissue-mimicking phantoms within a temperature-controlled water bath. We opted to conduct experiments in this well-controlled environment, rather than *in vivo*, so that any differences in acoustic behavior were attributable to the PFCnDs instead of slight changes to the experimental setup (e.g., differences between animals, changes in tissue stiffness, etc.). Future work should include testing these PFCnDs with different lipid shell compositions *in vivo* or in environments that better represent *in vivo* conditions, such as excised tissue, to validate that these differences in nanodroplet behavior are still exhibited *in vivo*. Additionally, as mentioned in Sec. III B, special care should be taken if using these PFCnDs for long-term studies with repeated injections to understand potential bioeffects caused by the presence of these nanodroplets *in vivo*.

IV. CONCLUSION

We investigated the influences of the lipid shell composition on the size distribution, ultrasound characteristics, and

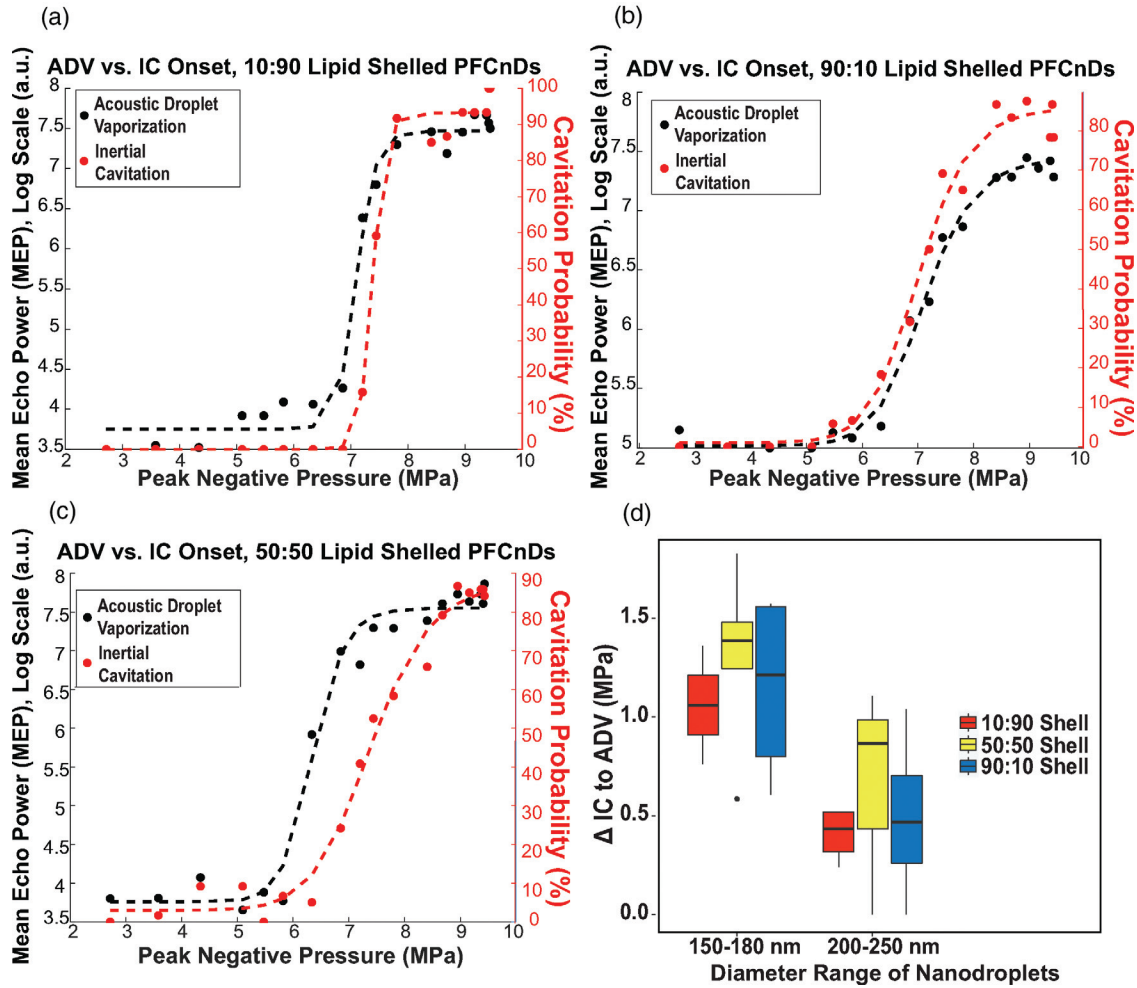


FIG. 6. ADV and IC onset of PFCnDs is influenced by their lipid shell composition. (a)–(c) Onset of ADV and IC for 10:90, 50:50, and 90:10 lipid shell PFCnDs with a 50:50 PFP:PFH perfluorocarbon core, respectively. These data are representative of all data sets collected. (d) The differential between ADV onset and IC onset of various lipid shell compositions of all PFC cores. This pressure differential is influenced by both shell composition and nanodroplet sizes.

vaporization dynamics of PFCnDs. Our results suggest that passing nanodroplets through a mesh filter yields nanodroplet suspensions with smaller average diameters by excluding large (450+ nm diameter) nanodroplets. Furthermore, lipid shell PFCnDs with a high proportion of PEGylated lipids have larger diameters, though the size distribution of nanodroplets may be more dependent on the fabrication method than lipid shell composition. PFCnDs with a 50:50 DPPC:DSPE-PEG₂₀₀₀ lipid shell composition created the strongest ultrasound contrast, had the longest duration in the phase-transitioned state, and had the greatest pressure difference between ADV onset and IC onset among all nanodroplet samples used in this study. Based on these results, the 50:50 lipid shelled PFCnDs are ideal candidates for theranostic applications and ultrasound imaging in general due to their monodispersity, high contrast-to-noise ratio, and large ADV-to-IC pressure differential. 90:10 and 10:90 lipid shelled PFCnDs are both excellent candidates for tissue ablation and localized drug delivery. Altering the perfluorocarbon core can influence the duration in which the PFCnD remains gaseous as well as the vaporization threshold of the

nanodroplets. The findings in this work can help guide researchers to fabricate PFCnDs with the desired ultrasonic properties for a variety of applications.

ACKNOWLEDGMENTS

We thank Eli Ricker of the Georgia Institute of Technology for helpful discussion and assistance with experimental setup. This work was supported by the National Science Foundation (Grant No. ECCS2102129) and the endowment of Georgia Institute of Technology.

Achmad, A., Yamaguchi, A., Hanaoka, H., and Tsushima, Y. (2018). “Thin-shelled PEGylated Perfluorooctyl bromide nanocapsules for tumor-targeted ultrasound contrast agent,” *Contrast Media Mol. Imaging* **2018**, 1725323.

Aliabouzar, M., Kumar, K. N., and Sarkar, K. (2019). “Effects of droplet size and perfluorocarbon boiling point on the frequency dependence of acoustic vaporization threshold,” *J. Acoust. Soc. Am.* **145**(2), 1105–1116.

Borden, M. A., Kruse, D. E., Caskey, C. F., Zhao, S., Dayton, P. A., and Ferrara, K. W. (2005). “Influence of lipid shell physicochemical properties on ultrasound-induced microbubble destruction,” *IEEE Trans. Ultrason. Ferroelectr. Freq. Control* **52**(11), 1992–2002.

- Cao, Y., Chen, Y., Yu, T., Guo, Y., Liu, F., Yao, Y., Li, P., Wang, D., Wang, Z., and Chen, Y. (2018). "Drug release from phase-changeable nanodroplets triggered by low-intensity focused ultrasound," *Theranostics* **8**(5), 1327–1339.
- Chattaraj, R., Goldscheiter, G. M., Yildirim, A., and Goodwin, A. P. (2016). "Phase behavior of mixed lipid monolayers on perfluorocarbon nanoemulsions and its effect on acoustic contrast," *RSC Adv.* **6**(112), 111318–111325.
- Chen, W.-S., Matula, T. J., Brayman, A. A., and Crum, L. A. (2003). "A comparison of the fragmentation thresholds and inertial cavitation doses of different ultrasound contrast agents," *J. Acoust. Soc. Am.* **113**(1), 643–651.
- de Gracia Lux, C., Vezeridis, A., Lux, J., Armstrong, A., Sirsi, S., Hoyt, K., and Mattrey, R. (2017). "Novel method for the formation of monodisperse superheated perfluorocarbon nanodroplets as activatable ultrasound contrast agents," *RSC Adv.* **7**(77), 48561–48568.
- de Jong, N., Frinking, P. J., Bouakaz, A., Goorden, M., Schourmans, T., Jingping, X., and Mastik, F. (2000). "Optical imaging of contrast agent microbubbles in an ultrasound field with a 100-MHz camera," *Ultrasound Med. Biol.* **26**(3), 487–492.
- Diaz, C., Benitez, C., Vidal, F., Barraza, L. F., Jiménez, V. A., Guzman, L., Fuentealba, J., Yevenes, G. E., and Alderete, J. B. (2018). "Cytotoxicity and *in vivo* plasma kinetic behavior of surface-functionalized PAMAM dendrimers," *Nanomed. Nanotechnol. Biol. Med.* **14**(7), 2227–2234.
- Errico, C., Pierre, J., Pezet, S., Desailly, Y., Lenkei, Z., Couture, O., and Tanter, M. (2015). "Ultrafast ultrasound localization microscopy for deep super-resolution vascular imaging," *Nature* **527**(7579), 499–502.
- Fabiilli, M. L., Haworth, K. J., Fakhri, N. H., Kripfgans, O. D., Carson, P. L., and Fowlkes, J. B. (2009). "The role of inertial cavitation in acoustic droplet vaporization," *IEEE Trans. Ultrason. Ferroelectr. Control* **56**(5), 1006–1017.
- Faez, T., Goertz, D., and Jong, N. D. (2011). "Characterization of Definity™ ultrasound contrast agent at frequency range of 5–15 MHz," *Ultrasound Med. Biol.* **37**(2), 338–342.
- Ferri, S., Wu, Q., De Grazia, A., Polydorou, A., May, J. P., Stride, E., Evans, N. D., and Carugo, D. (2021). "Tailoring the size of ultrasound responsive lipid-shelled nanodroplets by varying production parameters and environmental conditions," *Ultrason. Sonochem.* **73**, 105482.
- Goel, L., Wu, H., Zhang, B., Kim, J., Dayton, P. A., Xu, Z., and Jiang, X. (2021). "Nanodroplet-mediated catheter-directed sonothrombolysis of retracted blood clots," *Microsyst. Nanoeng.* **7**(1), 3.
- Goertz, D. E., de Jong, N., and van der Steen, A. F. (2007). "Attenuation and size distribution measurements of Definity™ and manipulated Definity™ populations," *Ultrasound Med. Biol.* **33**(9), 1376–1388.
- Goertz, D. E., Frijlink, M., Bouakaz, A., Chin, C., De Jong, N., and Van Der Steen, A. (2003). "The effects of bubble size on nonlinear scattering from microbubbles," in *Proceedings of the IEEE Symposium on Ultrasonics*, October 5–8, Honolulu, HI.
- Guo, S., Shi, A., Xu, S., Du, X., Wang, X., Zong, Y., Bouakaz, A., and Wan, M. (2017). "Lowering of acoustic droplet vaporization threshold via aggregation," *Appl. Phys. Lett.* **111**(25), 254102.
- Guo, X., Li, Q., Zhang, Z., Zhang, D., and Tu, J. (2013). "Investigation on the inertial cavitation threshold and shell properties of commercialized ultrasound contrast agent microbubbles," *J. Acoust. Soc. Am.* **134**(2), 1622–1631.
- Hannah, A. S., Luke, G. P., and Emelianov, S. Y. (2016). "Blinking phase-change nanocapsules enable background-free ultrasound imaging," *Theranostics* **6**(11), 1866–1876.
- Huynh, E., Leung, B. Y., Helfield, B. L., Shakiba, M., Gandier, J.-A., Jin, C. S., Master, E. R., Wilson, B. C., Goertz, D. E., and Zheng, G. (2015). "In situ conversion of porphyrin microbubbles to nanoparticles for multimodality imaging," *Nat. Nanotechnol.* **10**(4), 325–332.
- Ichihara, M., Shimizu, T., Imoto, A., Hashiguchi, Y., Uehara, Y., Ishida, T., and Kiwada, H. (2010). "Anti-PEG IgM response against PEGylated liposomes in mice and rats," *Pharmaceutics* **3**(1), 1–11.
- Ishida, T., Wang, X., Shimizu, T., Nawata, K., and Kiwada, H. (2007). "PEGylated liposomes elicit an anti-PEG IgM response in a T cell-independent manner," *J. Control. Release* **122**(3), 349–355.
- Ishijima, A., Tanaka, J., Azuma, T., Minamihata, K., Yamaguchi, S., Kobayashi, E., Nagamune, T., and Sakuma, I. (2016). "The lifetime evaluation of vapourised phase-change nano-droplets," *Ultrasonics* **69**, 97–105.
- Ishijima, A., Yamaguchi, S., Azuma, T., Kobayashi, E., Shibasaki, Y., Nagamune, T., and Sakuma, I. (2019). "Selective intracellular delivery of perfluorocarbon nanodroplets for cytotoxicity threshold reduction on ultrasound-induced vaporization," *Cancer Rep.* **2**(4), e1165.
- Ji, Y., Zheng, J., Geng, Z., Tan, T., Hu, J., Zhang, L., and Zhang, Y. (2022). "Controllable formation of bulk perfluorohexane nanodroplets by solvent exchange," *Soft Matter*. **18**, 425–433.
- Jing, B., Brown, M. E., Davis, M. E., and Lindsey, B. D. (2020). "Imaging the activation of low-boiling-point phase-change contrast agents in the presence of tissue motion using ultrafast inter-frame activation ultrasound imaging," *Ultrasound Med. Biol.* **46**(6), 1474–1489.
- Kang, S.-T., Lin, Y.-C., and Yeh, C.-K. (2014). "Mechanical bioeffects of acoustic droplet vaporization in vessel-mimicking phantoms," *Ultrason. Sonochem.* **21**(5), 1866–1874.
- Kawabata, K., Sugita, N., Yoshikawa, H., Azuma, T., and Umemura, S. (2005). "Nanoparticles with multiple perfluorocarbons for controllable ultrasonically induced phase shifting," *Jpn. J. Appl. Phys.* **44**(6S), 4548–4552.
- Kripfgans, O. D., Fabiilli, M. L., Carson, P. L., and Fowlkes, J. B. (2004). "On the acoustic vaporization of micrometer-sized droplets," *J. Acoust. Soc. Am.* **116**(1), 272–281.
- Kripfgans, O. D., Fowlkes, J. B., Miller, D. L., Eldevik, O. P., and Carson, P. L. (2000). "Acoustic droplet vaporization for therapeutic and diagnostic applications," *Ultrasound Med. Biol.* **26**(7), 1177–1189.
- Lensen, D., Gelderblom, E. C., Vriezema, D. M., Marmottant, P., Verdonshot, N., Versluis, M., De Jong, N., and Van Hest, J. C. (2011). "Biodegradable polymeric microcapsules for selective ultrasound-triggered drug release," *Soft Matter* **7**(11), 5417–5422.
- Lentacker, I., De Smedt, S. C., and Sanders, N. N. (2009). "Drug loaded microbubble design for ultrasound triggered delivery," *Soft Matter* **5**(11), 2161–2170.
- Li, D. S., Schneewind, S., Bruce, M., Khaing, Z., O'Donnell, M., and Pozzo, L. (2018). "Spontaneous nucleation of stable perfluorocarbon emulsions for ultrasound contrast agents," *Nano Lett.* **19**(1), 173–181.
- Li, H., Yang, Y., Zhang, M., Yin, L., Tu, J., Guo, X., and Zhang, D. (2018). "Acoustic characterization and enhanced ultrasound imaging of long-circulating lipid-coated microbubbles," *J. Ultrasound Med.* **37**(5), 1243–1256.
- Liu, J., Shang, T., Wang, F., Cao, Y., Hao, L., Ren, J., Ran, H., Wang, Z., Li, P., and Du, Z. (2017). "Low-intensity focused ultrasound (LIFU)-induced acoustic droplet vaporization in phase-transition perfluoropentane nanodroplets modified by folate for ultrasound molecular imaging," *Int. J. Nanomedicine* **12**, 911–923.
- Luke, G. P., Hannah, A. S., and Emelianov, S. Y. (2016). "Super-resolution ultrasound imaging *in vivo* with transient laser-activated nanodroplets," *Nano Lett.* **16**(4), 2556–2559.
- Matsunaga, T. O., Sheeran, P. S., Luois, S., Streeter, J. E., Mullin, L. B., Banerjee, B., and Dayton, P. A. (2012). "Phase-change nanoparticles using highly volatile perfluorocarbons: Toward a platform for extravascular ultrasound imaging," *Theranostics* **2**(12), 1185–1198.
- Mercado, K. P., Radhakrishnan, K., Stewart, K., Snider, L., Ryan, D., and Haworth, K. J. (2016). "Size-isolation of ultrasound-mediated phase change perfluorocarbon droplets using differential centrifugation," *J. Acoust. Soc. Am.* **139**(5), EL142–EL148.
- Mountford, P. A., and Borden, M. A. (2016). "On the thermodynamics and kinetics of superheated fluorocarbon phase-change agents," *Adv. Colloid Interface Sci.* **237**, 15–27.
- Mountford, P. A., Thomas, A. N., and Borden, M. A. (2015). "Thermal activation of superheated lipid-coated perfluorocarbon drops," *Langmuir* **31**(16), 4627–4634.
- Moyer, L. C., Timbie, K. F., Sheeran, P. S., Price, R. J., Miller, G. W., and Dayton, P. A. (2015). "High-intensity focused ultrasound ablation enhancement *in vivo* via phase-shift nanodroplets compared to microbubbles," *J. Ther. Ultrasound* **3**(1), 7.
- Niidome, T., Yamagata, M., Okamoto, Y., Akiyama, Y., Takahashi, H., Kawano, T., Katayama, Y., and Niidome, Y. (2006). "PEG-modified gold nanorods with a stealth character for *in vivo* applications," *J. Control. Release* **114**(3), 343–347.
- O'Reilly, M. A., and Hynynen, K. (2013). "A super-resolution ultrasound method for brain vascular mapping," *Med. Phys.* **40**(11), 110701.
- Paproski, R. J., Forbrich, A., Huynh, E., Chen, J., Lewis, J. D., Zheng, G., and Zemp, R. J. (2016). "Porphyrin nanodroplets: Sub-micrometer ultrasound and photoacoustic contrast imaging agents," *Small* **12**(3), 371–380.

- Pozzi, D., Colapicchioni, V., Caracciolo, G., Piovesana, S., Capriotti, A. L., Palchetti, S., De Grossi, S., Riccioli, A., Amenitsch, H., and Laganà, A. (2014). "Effect of polyethyleneglycol (PEG) chain length on the bio-nano-interactions between PEGylated lipid nanoparticles and biological fluids: From nanostructure to uptake in cancer cells," *Nanoscale* **6**(5), 2782–2792.
- Rapoport, N., Nam, K.-H., Gupta, R., Gao, Z., Mohan, P., Payne, A., Todd, N., Liu, X., Kim, T., and Shea, J. (2011). "Ultrasound-mediated tumor imaging and nanotherapy using drug loaded, block copolymer stabilized perfluorocarbon nanoemulsions," *J. Control. Release* **153**(1), 4–15.
- Reznik, N., Williams, R., and Burns, P. N. (2011). "Investigation of vaporized submicron perfluorocarbon droplets as an ultrasound contrast agent," *Ultrasound Med. Biol.* **37**(8), 1271–1279.
- Schad, K. C., and Hynynen, K. (2010). "In vitro characterization of perfluorocarbon droplets for focused ultrasound therapy," *Phys. Med. Biol.* **55**(17), 4933–4947.
- Schneider, M. (1999). "Characteristics of SonoVue™," *Echocardiography* **16**, 743–746.
- Seda, R., Li, D. S., Fowlkes, J. B., and Bull, J. L. (2015). "Characterization of bioeffects on endothelial cells under acoustic droplet vaporization," *Ultrasound Med. Biol.* **41**(12), 3241–3252.
- Şen, T., Tüfekçioğlu, O., and Koza, Y. (2015). "Mechanical index," *Anatol. J. Cardiol.* **15**(4), 334–336.
- Sheeran, P. S., Luois, S., Dayton, P. A., and Matsunaga, T. O. (2011). "Formulation and acoustic studies of a new phase-shift agent for diagnostic and therapeutic ultrasound," *Langmuir* **27**(17), 10412–10420.
- Sheeran, P. S., Wong, V. P., Luois, S., McFarland, R. J., Ross, W. D., Feingold, S., Matsunaga, T. O., and Dayton, P. A. (2011). "Decafluorobutane as a phase-change contrast agent for low-energy extravascular ultrasonic imaging," *Ultrasound Med. Biol.* **37**(9), 1518–1530.
- Sheng, D., Deng, L., Li, P., Wang, Z., and Zhang, Q. (2021). "Perfluorocarbon nanodroplets with deep tumor penetration and controlled drug delivery for ultrasound/fluorescence imaging guided breast cancer therapy," *ACS Biomater. Sci. Eng.* **7**(2), 605–616.
- Shpak, O., Verweij, M., Vos, H. J., de Jong, N., Lohse, D., and Versluis, M. (2014). "Acoustic droplet vaporization is initiated by superharmonic focusing," *Proc. Natl. Acad. Sci. U.S.A.* **111**(5), 1697–1702.
- Song, P., Trzasko, J. D., Manduca, A., Huang, R., Kadirvel, R., Kallmes, D. F., and Chen, S. (2018). "Improved super-resolution ultrasound microvessel imaging with spatiotemporal nonlocal means filtering and bipartite graph-based microbubble tracking," *IEEE Trans. Ultrason. Ferroelectr. Freq. Control* **65**(2), 149–167.
- Suzuki, T., Ichihara, M., Hyodo, K., Yamamoto, E., Ishida, T., Kiwada, H., Ishihara, H., and Kikuchi, H. (2012). "Accelerated blood clearance of PEGylated liposomes containing doxorubicin upon repeated administration to dogs," *Int. J. Pharm.* **436**(1-2), 636–643.
- Ullmann, C., Babick, F., and Stintz, M. (2019). "Microfiltration of submicron-sized and nano-sized suspensions for particle size determination by dynamic light scattering," *Nanomaterials* **9**(6), 829–844.
- Verhoef, J. J., and Anchordoquy, T. J. (2013). "Questioning the use of PEGylation for drug delivery," *Drug Deliv. Transl. Res.* **3**(6), 499–503.
- Viitala, L., Pajari, S., Gentile, L., Määttä, J., Gubitosi, M., Deska, J., Sammalkorpi, M., Olsson, U., and Murtomäki, L. (2019). "Shape and phase transitions in a PEGylated phospholipid system," *Langmuir* **35**(11), 3999–4010.
- Williams, R., Wright, C., Cherin, E., Reznik, N., Lee, M., Gorelikov, I., Foster, F. S., Matsuura, N., and Burns, P. N. (2013). "Characterization of submicron phase-change perfluorocarbon droplets for extravascular ultrasound imaging of cancer," *Ultrasound Med. Biol.* **39**(3), 475–489.
- Wu, Q., Mannaris, C., May, J. P., Bau, L., Polydorou, A., Ferri, S., Carugo, D., Evans, N. D., and Stride, E. (2021). "Investigation of the acoustic vaporization threshold of lipid-coated perfluorobutane nanodroplets using both high-speed optical imaging and acoustic methods," *Ultrasound Med. Biol.* **47**(7), 1826–1843.
- Xiang, Y., Bernards, N., Hoang, B., Zheng, J., and Matsuura, N. (2019). "Perfluorocarbon nanodroplets can reoxygenate hypoxic tumors in vivo without carbogen breathing," *Nanotheranostics* **3**(2), 135–144.
- Xu, S., Chang, N., Wang, R., Liu, X., Guo, S., Wang, S., Zong, Y., and Wan, M. (2018). "Acoustic droplet vaporization and inertial cavitation thresholds and efficiencies of nanodroplets emulsions inside the focused region using a dual-frequency ring focused ultrasound," *Ultrason. Sonochem.* **48**, 532–537.
- Yarmoska, S. K., Yoon, H., and Emelianov, S. Y. (2019). "Lipid shell composition plays a critical role in the stable size reduction of perfluorocarbon nanodroplets," *Ultrasound Med. Biol.* **45**(6), 1489–1499.
- Yin, T., Wang, P., Zheng, R., Zheng, B., Cheng, D., Zhang, X., and Shuai, X. (2012). "Nanobubbles for enhanced ultrasound imaging of tumors," *Int. J. Nanomedicine* **7**, 895–904.
- Yoo, K., Walker, W. R., Williams, R., Tremblay-Darveau, C., Burns, P. N., and Sheeran, P. S. (2018). "Impact of encapsulation on in vitro and in vivo performance of volatile nanoscale phase-shift perfluorocarbon droplets," *Ultrasound Med. Biol.* **44**(8), 1836–1852.
- Yoon, H., Hallam, K. A., Yoon, C., and Emelianov, S. Y. (2018). "Super-resolution imaging with ultrafast ultrasound imaging of optically triggered perfluorohexane nanodroplets," *IEEE Trans. Ultrason. Ferroelectr. Freq. Control* **65**(12), 2277–2285.
- Yu, J., Chen, X., Villanueva, F. S., and Kim, K. (2016). "Vaporization and recondensation dynamics of indocyanine green-loaded perfluoropentane droplets irradiated by a short pulse laser," *Appl. Phys. Lett.* **109**(24), 243701.
- Yu, J., Lavery, L., and Kim, K. (2018). "Super-resolution ultrasound imaging method for microvasculature in vivo with a high temporal accuracy," *Sci. Rep.* **8**(1), 13918.